Electronic Supplementary Material (ESI) for CrystEngComm.


# A (4,6)-c copper-organic framework constructed from triazole-inserted dicarboxylate linker with $CO_2$ selective adsorption

Hong-Xin Li,[ab] Zong-Hui Zhang,[b] Han Fang,[b] Xin-Ai Guo,[b] Guo-Tong Du,[b] Qin Wang,[a] Dong-Xu Xue*[b]

[a] Shaanxi Key Laboratory of Low Metamorphic Coal Clean Utilization, School of Chemistry and Chemical Engineering, Yulin University, Yulin, 719000, China.
[b] Key Laboratory of Applied Surface and Colloid Chemistry, Ministry of Education, Key Laboratory of Organometallic Material Chemistry, School of Chemistry & Chemical Engineering, Shaanxi Normal University, Xi'an 710062, China.
E-mail: xuedx@snnu.edu.cn

## Table of Contents

## 1. Materials and General Procedures

All reagents were obtained from commercial sources and used without further purification. PXRD measurements were performed on a Bruker D8 Advance diffractometer with Cu *Kα* ($\lambda$ = 1.5406 Å), and the X-ray tube was operated at 40 kV and 40 mA. High-resolution thermogravimetric analysis (TGA) was performed under a continuous $N_2$ flow and recorded on a Q600SDT thermal analyzer with a heating rate of 5 °C/min. Elemental analyses (C, H, and N) was obtained from a Vario EL cube analyzer. Fourier transform infrared (FT-IR) spectrum (400-4000 $cm^{-1}$, KBr pellet) was collected in the solid state on a Bruker Tensor 27 FT-IR spectrometer. X-ray photoelectron spectroscopy (XPS) was used AXIS ULTRA with an Al Kα microfocused X-ray source and the C 1s peak at 284.8 eV as internal standard.

**Synthesis of Cu-TZDB**

A mixture of $Cu(NO_3)_2{\cdot}3H_2O$ (21.0 mg, 0.087 mmol), $H_2$TZDB (6.7 mg, 0.02175 mmol), DMF (1.0 mL), methanol (0.5 mL) and acetic acid (40 μL) were combined in a 20 mL scintillation vial, sealed and heated to 85 °C for 36 h. The blue and hexagonal prism shaped crystals were collected, washed with DMF, and then air-dried. Yield ≈ 46% (based on ligand). Selected IR (KBr, $cm^{-1}$): 3455 (br), 3050 (w), 2927 (w), 1660 (s), 1612 (w), 1553 (s), 1391 (vs), 1284 (w), 1252 (w), 1179 (m), 1101 (m), 1015 (m), 872 (m), 845 (m), 794 (m), 750 (s), 702 (w), 664 (m), 561 (w). Elem. Anal. (%) $[Cu_2(C_{16}H_8N_3O_4)(CH_3COO^-)(H_2O)_2]{\cdot}[Cu(CH_3COO^-)_2{\cdot}(H_2O)(C_3H_7NO)_5]$ Calcd. C, 40.64; H, 5.35; N, 10.25. Found: C, 40.71; H, 4.68; N, 10.71.

## 2. X-ray Photoelectron Spectroscopy

XPS characterization were employed to obtain further information about the oxidation state of Cu in Cu-TZDB. XPS core level spectra of the Cu 2d region shown in Figure S1, the peaks at 933 and 953 eV are ascribed to CuII, indicating the existence of CuII in Cu-TZDB.

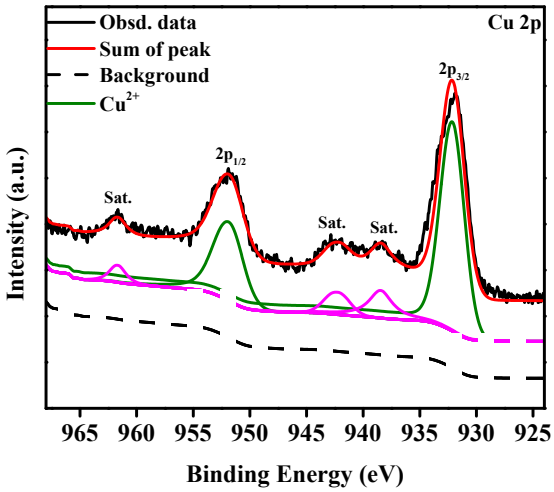


**Fig. S1** XPS pattern of Cu-TZDB.

## 3. Additional Structural Figures

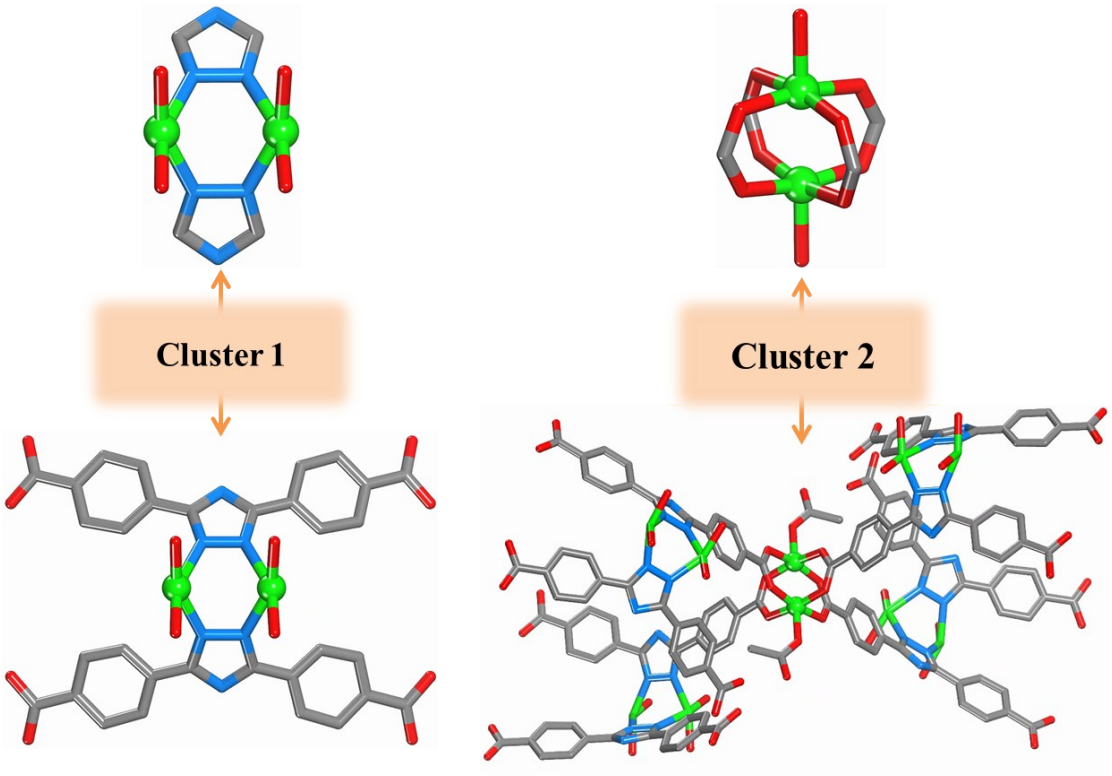


**Fig. S2** Schematic representation of the two types clusters in Cu-TZDB and their chemical environment. Cu = green, C = gray, N = blue and O = red. Hydrogen atoms are omitted for clarity.

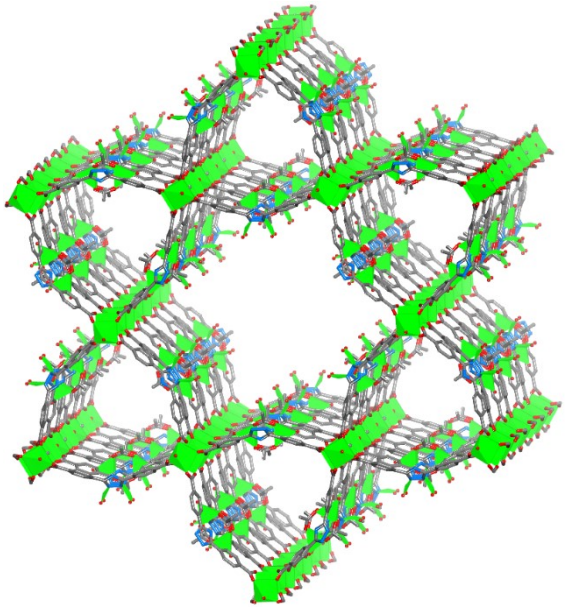

**Fig. S3** Schematic representation of Cu-TZDB contain the guest molecules of $[Cu(Ac)_2(H_2O)]$.

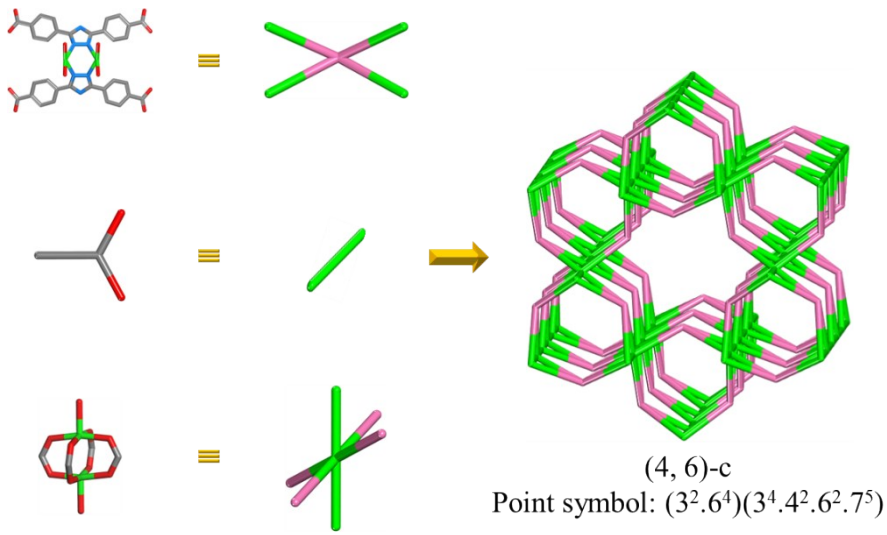


**Fig. S4** The topology analysis of Cu-TZDB in node−linker strategy.

## 4. Powder X-ray Diffraction (PXRD) Patterns

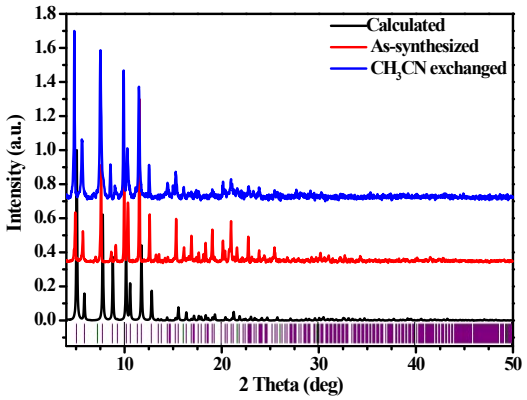


**Fig. S5** PXRD patterns of Cu-TZDB.

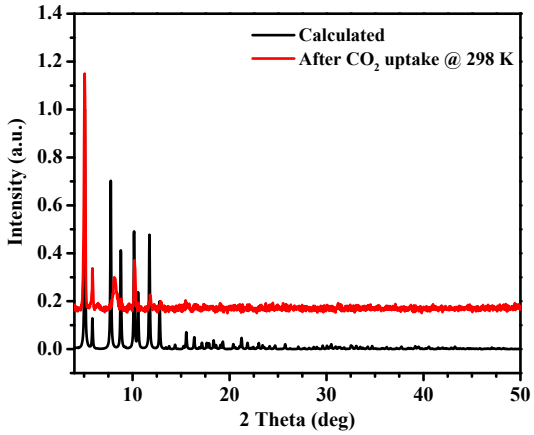


**Fig. S6** PXRD pattern of Cu-TZDB sample after $CO_2$ uptake test at 298 K.

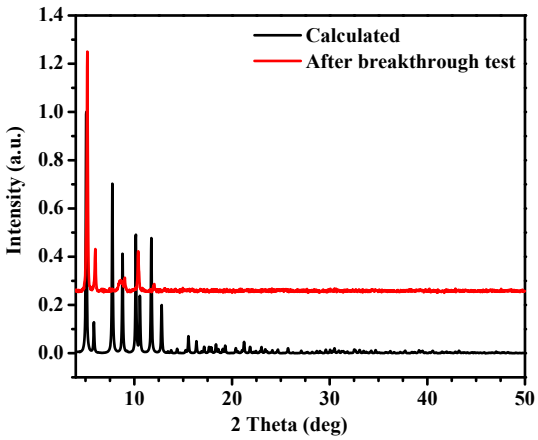


**Fig. S7** PXRD pattern of Cu-TZDB sample after breakthrough test at 298 K and 1 bar.

## 5. Thermal Gravimetric Analysis (TGA)

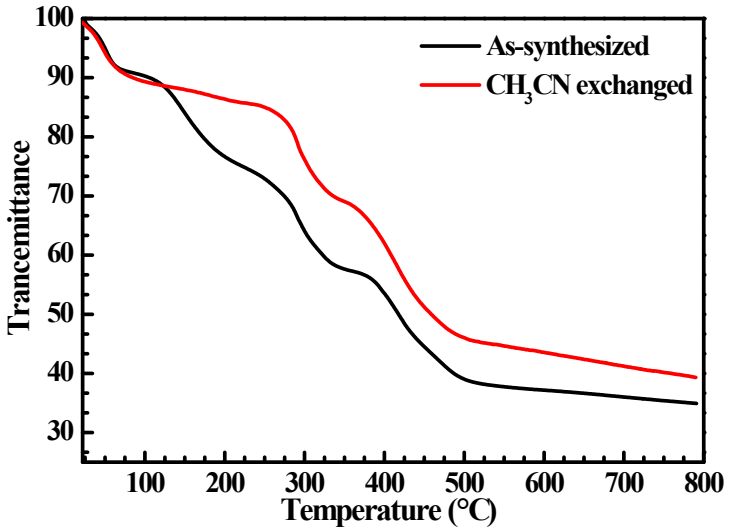


**Fig. S8** TGA plots of the as-synthesized and solvent-exchanged Cu-TZDB.

## 6. Low-Pressure Gas Sorption Measurements

Low pressure gas sorption studies were conducted on a fully automated micropore gas analyzer Autosorb-iQ3 (Quantachrome Instruments) at relative pressures up to 1 atm. The cryogenic temperature was controlled by liquid nitrogen at 77 K. The bath temperature for the $CO_2$, $CH_4$, and $N_2$ sorption measurements was controlled by a recirculating bath containing an ethylene glycol/water mixture. The apparent surface area was calculated from the nitrogen adsorption isotherm collected at 77 K by applying the BET models. Pore size distribution analyses was performed using a cylindrical/spherical NLDFT pore model system by assuming an oxidic (zeolitic) surface.

**The calculation of adsorption enthalpy:**

Adsorption enthalpy ($Q_{st}$) was determined by fitting the adsorption isotherms at 273 and 298 K to the virial 2 equation (Eqn 1);

$$lnP = \ln(N) + (\frac{1}{T})\sum_{i=0}^{m} a_i \times N_i + \sum_{j=0}^{n} b_i \times N_i \qquad (1)$$

Where $N$ is the amount of gas adsorbed in mmol/g, $P$ is the pressure in Pa, $a_i$ and $b_j$ are the empirical constants, and $T$ is the temperature in K.

Using the virial 2 equation fit, the isosteric heat of adsorption can be calculated for Cu-TZDB as a function of the total amount of gas adsorbed using the Clausius-Clapeyron equation (Eqn 2).

$$\frac{dlnp}{dT} = \frac{\Delta H}{nRT^2} = \frac{\Delta_r H_m}{RT^2} \qquad (2)$$

**The calculation of IAST selectivity:**

IAST (Ideal Adsorption Solution Theory) was used to predict binary mixture adsorption from the experimental pure gas isotherms.[1-3] In order to perform the integrations required by IAST, the single-component isotherms should be fitted by a proper model. In fact, several methods to do this are available. We found for this set of data that the dual-site Langmuir-Freundlich (DSLF) equation (Eqn 3) was successful in fitting the data. As can be seen in Fig. S12 and Table S1, the model fits the isotherms very well.

$$q = \frac{q_{m,1} b_1 p^{1/n_1}}{1 + b_1 p^{1/n_1}} + \frac{q_{m,2} b_2 p^{1/n_2}}{1 + b_2 p^{1/n_2}} \quad \text{(Eqn 3)}$$

Herein, $P$ is the pressure of the bulk gas at equilibrium with the adsorbed phase (kPa), $q$ is the adsorbed amount per mass of adsorbent (mmol/g), $q_{m,1}$ and $q_{m,2}$ are the saturation capacities of sites 1 and 2 (mmol/g), $b_1$ and $b_2$ are the affinity coefficients of sites 1 and 2 (1/kPa), and $n_1$ and $n_2$ represent the deviations from an ideal homogeneous surface. The fitted parameters were then used to predict multicomponent adsorption with IAST.

The selectivity $S_{A/B}$ in a binary mixture of components A and B is defined as $(x_A/y_A)/(x_B/y_B)$, where $x_i$ and $y_i$ are the mole fractions of component $i$ ($i$ = A, B) in the adsorbed and bulk phases, respectively.

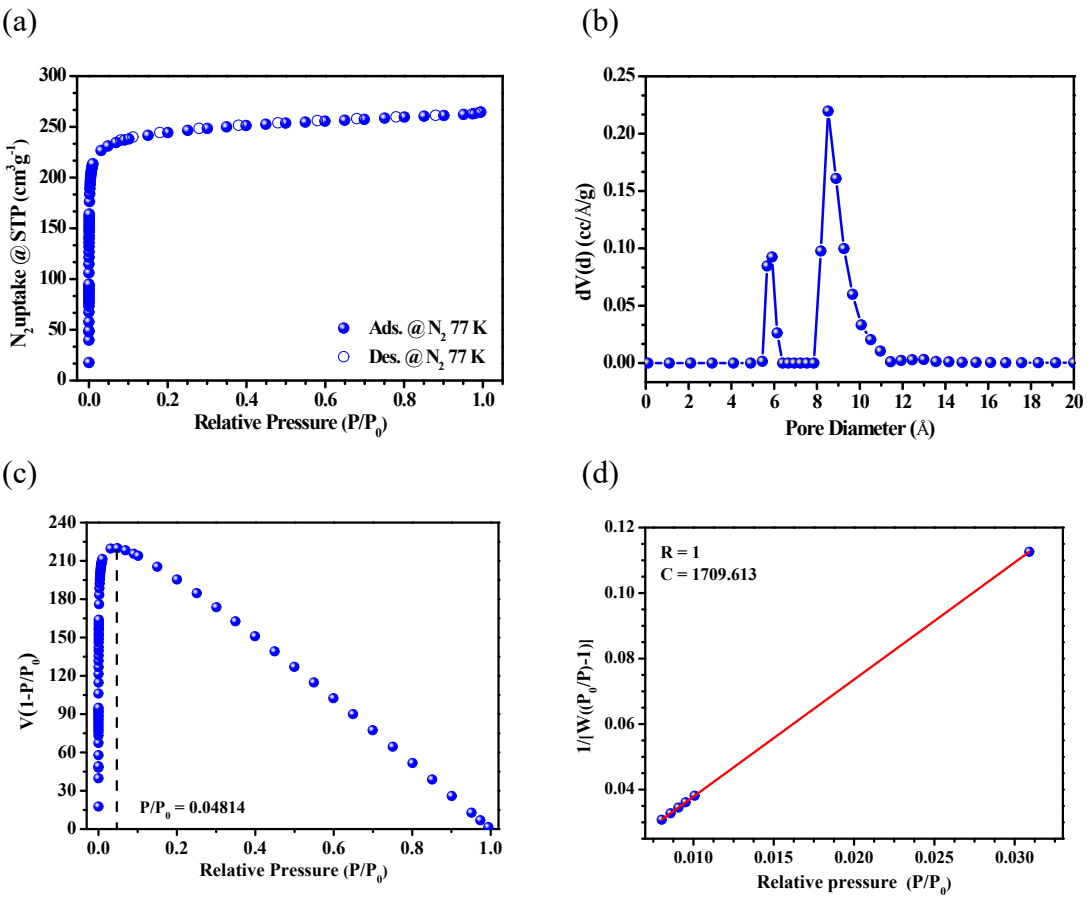


**Fig. S6** (a) Adsorption (closed)/desorption (open) isotherms and (b) pore size distribution of Cu-TZDB, (c) $V(1-P/P_0)$ vs. $P/P_0$ for Cu-TZDB, only the range below $P/P_0 = 0.048$ satisfies the first consistency criterion for applying the BET theory and (d) plot of the linear region for the BET equation.

(a)

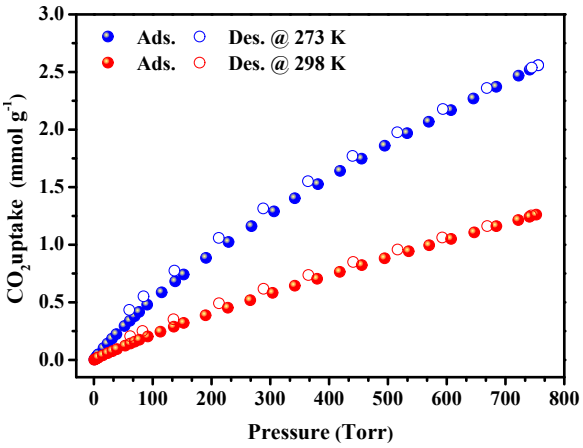
Ads.
Des. @ 273 K
Ads.
Des. @ 298 K
CO2 uptake (mmol g-1)
Pressure (Torr)

(b)

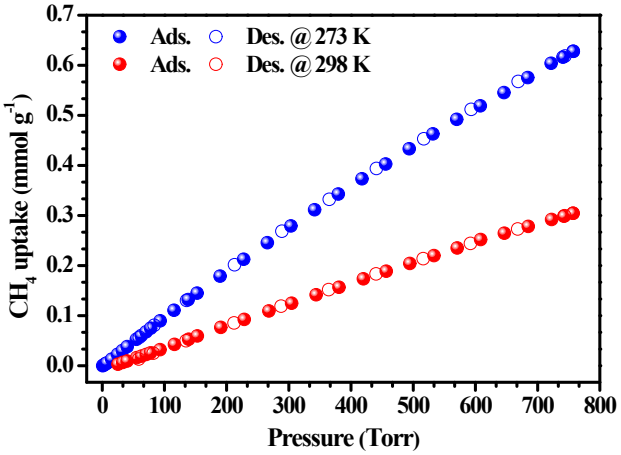
Ads.
Des. @ 273 K
Ads.
Des. @ 298 K
CH4 uptake (mmol g-1)
Pressure (Torr)

(c)

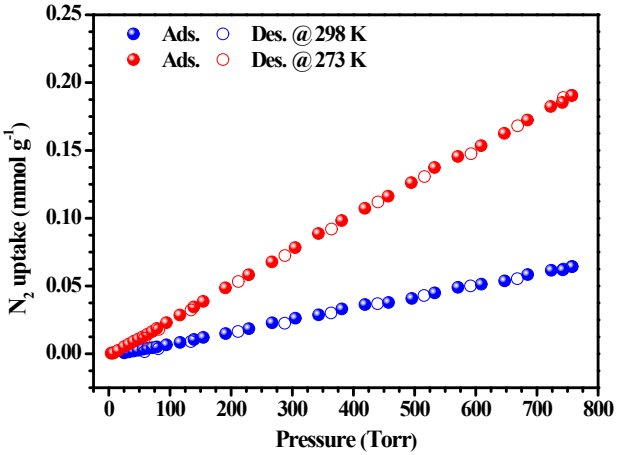
Ads.
Des. @ 298 K
Ads.
Des. @ 273 K
N2 uptake (mmol g-1)
Pressure (Torr)

**Fig. S10** Pure component sorption isotherms of different gases for Cu-TZDB at 273 and 298 K, respectively.

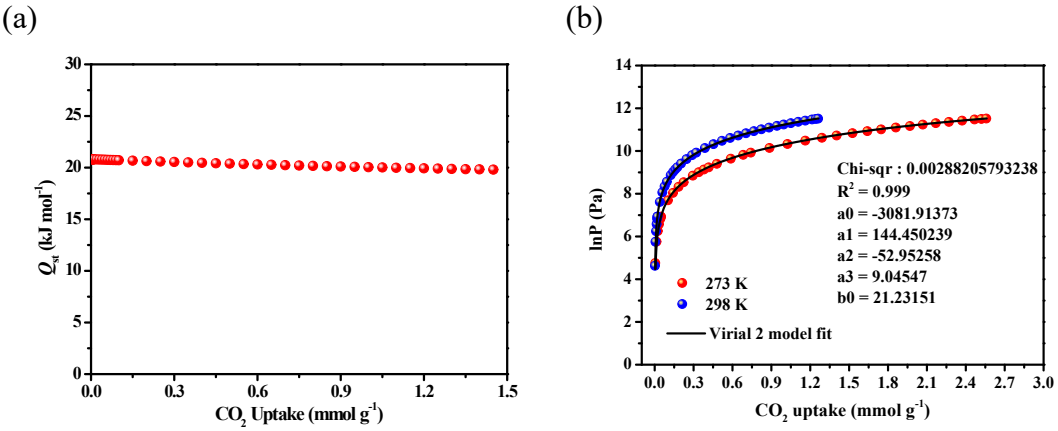


**Fig. S11** (a) The $Q_{st}$ of $CO_2$ for Cu-TZDB, (b) virial 2 model fitting (lines) of $CO_2$ adsorption isotherms (points) for Cu-TZDB measured at 273 and 298 K.

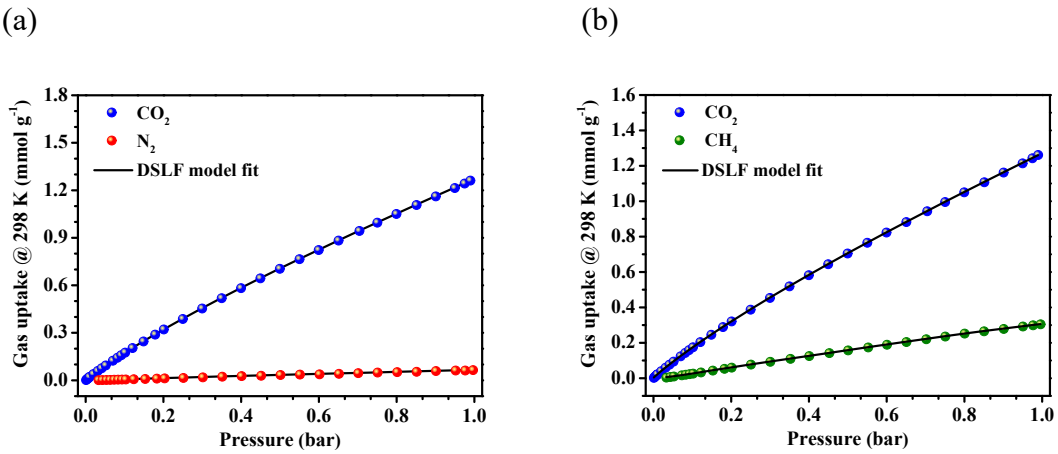


**Fig. S12** Dual-site Langmuir-Freundlich (DSLF) equation fits (lines) and adsorption isotherms (points) of different gases at 298 K for Cu-TZDB.

**Table S1.** DSLF equation fitting parameters of different gas adsorption isotherms for Cu-TZDB.

| Gases | $CO_2$ | $N_2$ | $CH_4$ |
|---|---|---|---|
| $q_{m,1}$ | 2.90263369138811 | 0.0129885174527399 | 0.521594311168253 |
| $q_{m,2}$ | 1.06739966823609 | 0.103124344993167 | 0.0836979179328822 |
| $b_1$ | 0.00841369842374762 | 3.53581298774148E-15 | 0.000105459066514516 |
| $b_2$ | 0.0000186871214841563 | 0.00205431050216329 | 0.00628764096776589 |
| $n_1$ | 0.948553447932081 | 7.34359338740143 | 1.92691224404176 |
| $n_2$ | 2.16188461493806 | 1.3803407120793 | 1.68639364749735 |
| *Reduced Chi-Sqr* | 0.000806517683236324 | 0.000196191564715609 | 0.000272980769411093 |
| $R^2$ | 0.999993371905339 | 0.999482236465518 | 0.999973547934417 |

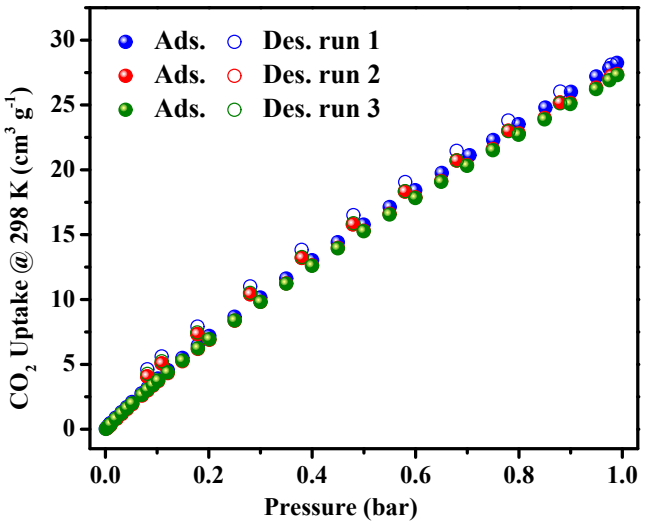


**Fig. S13** Repeated measurements of $CO_2$ uptake isotherms for Cu-TZDB at 298 K.

**Table S2.** The $CO_2/N_2$ selectivity and $CO_2$ enthalpy of some investigated MOF materials and Cu-TZDB.

| MOF | $Q_{st}$ (kJ/mol) | Selectivity ($CO_2/N_2$ = 15/85) | T (K) | Ref. |
|---|---|---|---|---|
| SIFSIX-3-Zn | - | 1818 | 298 | 4 |
| SIFSIX-2-Cu-i | 31.9 | 140 | 298 | |
| SIFSIX-2-Cu | 22 | 11.3 | 298 | |
| NJU-Bai52 | 44.2 | 581 | 298 | 5 |
| $Zn_2(bpdc)_2(bpee)$ | 28.5 | 493.8 | 298 | 6 |
| mmen-CuBTTri | 96 | 327 | 298 | 7 |
| UTSA-16 | 34.6 | 314.7 | 296 | 8 |
| Mg-MOF-74 | 42 | 182.1 | 296 | 9 |
| HKUST-1 | — | 101[a] | 298 | 10 |
| NJU-Bai21 | 22.2 | 93 | 298 | 11 |
| NJU-Bai22 | 25.6 | 81 | 298 | |
| NJU-Bai23 | 25.1 | 72 | 298 | |
| LIFM-11(Cu) | 53 | 81.9 | 298 | 12 |
| FJUT-4 | 35.2 | 69.3 | 298 | 13 |
| UTSA-85a | 22.0 | 62.5 | 296 | 14 |
| Y-bptc | 24 | 62 | 298 | 15 |
| HNUST-1 | 31.2 | 39.8 | 298 | 16 |

| | | | | |
|---|---|---|---|---|
| SYSU | 28.2 | 34.2 | 298 | 17 |
| PCN-61 | 22 | 14.7 | 298 | 18 |
| Bio-MOF-11 | 45 | 65 | 298 | 19, 20 |
| $[Cu(bpy\text{-}1)_2(SiF_6)]$ | 27 | 17.5 | 298 | 21 |
| Cu-TZDB | 20.8 | 171.3 ($CO_2/N_2$ = 20/80) | 298 | This work |

[a]Selectivity from Henry's Law.

## 7. Breakthrough Tests

The transient breakthrough tests were carried out in homemade HPMC41 gas separation test system (Nanjing Hope Analytical Equipment Co., Ltd) (Fig. S10). The flow rates of all gases are regulated by mass flow controllers, and the effluent gas stream from the column is monitored by a gas chromatography (GC). In this test, 548.8 mg of Cu-TZDB sorbent was ground and packed into a stainless-steel column (12 cm length × 0.30 cm internal diameter) with silica wool filling the void space. The sorbent was activated *in situ* in the column before the temperature of the column was decreased to 298 K. The packed column was initially purged with He for 30 min until no other gases were detected in the effluent. Then, dry gas mixture of $CO_2/N_2$ flow at 2 mL $min^{-1}$ (20/80, v/v) and $CO_2/CH_4$ flow at 2 mL $min^{-1}$ (50/50, v/v) were dosed into the column, respectively. The dead volume was determined using the same column after adsorption saturation. The absolute adsorbed amount of gas $i$ ($q_i$) is calculated from the breakthrough curve by the equation according literature with modification:[22] (Eqn 4):

$$q_i = \frac{F_i \times t_0 - V_{dead} - \int_0^{t_0} F_e \Delta t}{m} \quad (4)$$

where $F_i$ is the influent flow rate of the specific gas ($cm^3$ $min^{-1}$); $t_0$ is the adsorption time (min); $V_{dead}$ is the dead volume of the system ($cm^3$); $F_e$ is the effluent flow rate of the specific gas ($cm^3$ $min^{-1}$); and $m$ is the mass of the sorbent (g). The selectivity of the breakthrough experiment is defined as:

$$\alpha = (q_1/y_1)/(q_2/y_2) \quad (5)$$

Where $y_i$ is the molar fraction of gas $i$ in the gas mixture. The same breakthrough experiments were repeated three times after the adsorbent saturated with $CO_2$ was regenerated by a pure He flow.

**Table S3.** The summary of the absolute adsorbed amount of $CO_2$ ($q$) and the selectivity ($\alpha$) of breakthrough test.

| | $CO_2/N_2$ = 20/80 | | $CO_2/CH_4$ = 50/50 | |
|---|---|---|---|---|
| | $q_{CO_2}$ (cm³/g) | $\alpha$ | $q_{CO_2}$ (cm³/g) | $\alpha$ |
| Cu-TZDB | 5.2 | 2.6 | 9.80 | 1.9 |


**Fig. S14** The homemade HPMC41 gas separation test system.

## 8. Single Crystal X-ray Crystallography Data

Single-crystal X-ray diffraction data for Cu-TZDB were collected on a Bruker D8 venture diffractometer at 153 K using graphite monochromated $Cu_{Ka}$ radiation ($\lambda$ = 1.5418 Å). Indexing was performed using APEX3 (Difference Vectors method).[23] Data integration and reduction were performed using SaintPlus 6.01.[24] Absorption correction was performed by multi-scan method implemented in SADABS.[25] Space group was determined using XPREP implemented in APEX3. The structure was solved by direct method and refined with full-matrix least squares technique using the SHELXT[26] package or refined using SHELXL-2014 (full-matrix least-squares on $F^2$) contained in Olex2.[27] Non-hydrogen atoms were refined with anisotropic displacement parameters during the final cycles. Hydrogen atoms were located at geometrically calculated positions to their carrier atoms and refined with isotropic thermal parameters included in the final stage of the refinement.

A summary of the crystallographic data is given in Table S4. CCDC 2243167 (Cu-TZDB) contains the supplementary crystallographic data for this paper. The data can be obtained free of charge from The Cambridge Crystallographic Data Centre.

**Table S4.** Crystal data and refinement results for Cu-TZDB.

| **Identification code** | **Cu-TZDB** |
|---|---|
| Empirical formula | $C_{42}H_{31}Cu_6N_6$ |
| Formula weight | 1384.97 |
| Temperature/K | 153.0 |
| Wavelength/Å | 1.54178 |
| Crystal system | Hexagonal |
| Space group | $P6_3/mmc$ |
| Unit cell dimensions/Å | $a$ = 34.8261(6)<br>$c$ = 17.3791(4) |
| Volume/Å$^3$ | 18254.4(8) |
| Z | 6 |
| Density (calculated)/Mg/m$^3$ | 0.756 |
| Absorption coefficient/mm$^{-1}$ | 1.477 |
| F (000) | 4146.0 |
| Crystal size/mm$^3$ | 0.30 x 0.15 x 0.15 |
| Theta range for data collection/° | 2.93 to 63.353 |
| Index ranges | -34<=h<=39<br>-40<=k<=24<br>-19<=l<=15 |
| Reflections collected | 51185 |

| | |
|---|---|
| Independent reflections | 5413 [$R$(int) = 0.0501] |
| Completeness to theta = 63.353° | 99.4% |
| Refinement method | Full-matrix least-squares on $F^2$ |
| Data / restraints / parameters | 5413 / 38 / 183 |
| Goodness-of-fit on $F^2$ | 1.790 |
| Final $R$ indices [$I$>2sigma($I$)] | $R_1$ = 0.1401, $wR_2$ = 0.4080 |
| $R$ indices (all data) | $R_1$ = 0.1682, $wR_2$ = 0.4432 |
| Largest diff. peak and hole/e.Å$^{-3}$ | 2.58 and -1.13 |

## 9. Topology Analysis Results

Structure #1 - "Cu-TZDB".
Structure of dimension 3.
Given space group is $P6_3/mmc$.
12 nodes and 30 edges in repeat unit as given.
Given repeat unit is accurate.
Point group has 24 elements.
2 kinds of node.
Coordination sequences:
Node 1: 6 14 36 58 104 150 216 266 364 424
Node 2: 4 14 28 56 84 148 182 274 306 458
TD10 = 1597.0000
Ideal space group is $P6_3/mmc$.
Structure is new for this run.

Relaxed cell parameters:
a = 3.46755, b = 3.46755, c = 1.99701
alpha = 90.0000, beta = 90.0000, gamma = 120.0000
Cell volume: 20.79488
Relaxed positions:
Node 1: 0.00000 0.50000 0.00000
Node 2: 0.50009 0.25004 0.25000
Edges:
0.00000 0.50000 0.00000 <-> 0.25004 0.50009 -0.25000
0.00000 0.50000 0.00000 <-> 0.00000 0.50000 0.50000
Edge centers:
0.12502 0.50004 -0.12500
0.00000 0.50000 0.25000

Edge statistics: minimum = 0.99851, maximum = 1.00037, average = 1.00000
Angle statistics: minimum = 51.32259, maximum = 180.00000, average = 111.42565
Shortest non-bonded distance = 0.86642
Degrees of freedom: 3
Finished structure #1 - "Cu-TZDB".

## 10. References


1. A. L. Myers, J. M. Prausnitz, *AIChE J.*, 1965, **11**, 121-127.
2. Y. S. Bae, K. L. Mulfort, H. Frost, P. Ryan, S. Punnathanam, L. J. Broadbelt, J. T. Hupp, R. Q. Snurr, *Langmuir*, 2008, **24**, 8592-8598.
3. B. Mu, F. Li, K. S. Walton, *Chem. Commun.*, 2009, 2493-2495.
4. P. Nugent, Y. Belmabkhout, S. D. Burd, A. J. Cairns, R. Luebke, K. Forrest, T. Pham, S. Ma, B. Space, L. Wojtas, M. Eddaoudi and M. J. Zaworotko, *Nature*, 2013, **495**, 80-84.
5. X. Song, M. Zhang, C. Chen, J. Duan, W. Zhang, Y. Pan and J. Bai, *J. Am. Chem. Soc.*, 2019, **141**, 14539-14543.
6. H. Wu, R. S. Reali, D. A. Smith, M. C. Trachtenberg and J. Li, *Chem. Eur. J.*, 2010, **16**, 13951-13954.
7. T. M. McDonald, D. M. D'Alessandro, R. Krishnac and J. R. Long, *Chem. Sci.*, 2011, **2**, 2022-2028.
8. S. Xiang, Y. He, Z. Zhang, H. Wu, W. Zhou, R. Krishna and B. Chen, *Nat. Commun.*, 2012, **3**, 954-961.
9. S. R. Caskey, A. G. Wong-Foy and A. J. Matzger, *J. Am. Chem. Soc.*, 2008, **130**, 10870-10871.
10. Z. Zhang, Y. Zhao, Q. Gong, Z. Lib and J. Li, *Chem. Commun.*, 2013, **49**, 653-661.
11. Z. Lu, J. Bai, ChengHang, F. Meng, W. Liu, Y. Pan and X. You, *Chem. Eur. J.*, 2016, **22**, 6277-6285.
12. Y. Xiong, Y.-Z. Fan, R. Yang, S. Chen, M. Pan, J.-J. Jiang and C.-Y. Su, *Chem. Commun.*, 2014, **50**, 14631-14634.
13. L. Zhang, S. Lin, Y. Liu, X. Zeng, J. You, T. Xiao, Y. Feng, Z. He, S. Chen, N. Hua, X. Ye, Z.-W. Wei and C.-X. Chen, *Inorg. Chem.*, 2023, **62**, 8058-8063.

14. O. Alduhaish, H. Wang, B. Li, H. D. Arman, V. Nesterov, K. Alfooty and B. Chen, *ChemPlusChem*, 2016, **81**, 1-7.
15. C. He, P. Zhang, S. Ma, Y. Zhang and T. Hu, *Dalton Trans.*, 2023, **52**, 7975-7981.
16. B. Zheng, H. Liu, Z. Wang, X. Yu, P. Yi and J. Bai, *CrystEngComm.*, 2013, **15**, 3517-3520.
17. L. Du, Z. Lu, K. Zheng, J. Wang, X. Zheng, Y. Pan, X. You and J. Bai, *J. Am. Chem. Soc.*, 2013, **135**, 562-565.
18. B. Zheng, J. Bai, J. Duan, L. Wojtas and M. J. Zaworotko, *J. Am. Chem. Soc.*, 2011, **133**, 748-751.
19. K. Sumida, D. L. Rogow, J. A. Mason, T. M. McDonald, E. D. Bloch, Z. R. Herm, T.-H. Bae and J. R. Long, *Chem. Rev.*, 2012, **112**, 724-781.
20. R. Poloni, K. Lee, R. F. Berger, B. Smit and J. B. Neaton, *J. Phys. Chem. Lett.*, 2014, **5**, 861-865.
21. S. D. Burd, S. Ma, J. A. Perman, B. J. Sikora, R. Q. Snurr, P. K. Thallapally, L. W. Jian Tian and M. J. Zaworotko, *J. Am. Chem. Soc.*, 2012, **134**, 3663-3666.
22. Y. Zhao, K. X. Yao, B. Teng, T. Zhang, Y. Han, *Energy Environ. Sci.* 2013, **6**, 3684-3692.
23. Bruker APEX2; Bruker AXS, Inc.: Madison, WI, 2010.
24. Bruker SAINT, Data Reduction Software; Bruker AXS, Inc.: Madison, WI, 2009.
25. G. M. Sheldrick, University of Gottingen: Gottingen, Germany, 1996.
26. G. M. Sheldrick, *Acta Crystallogr.*, 2015, **A71**, 3-8.
27. O. V. Dolomanov, L. J. Bourhis, R. J. Gildea, J. A. K. Howard, H. Puschmann, *J. Appl. Crystallogr.*, 2009, **42**, 339-341.